Tucholke, B.E., Sibuet, J.-C., and Klaus, A. (Eds.)
Proceedings of the Ocean Drilling Program, Scientific Results Volume 210

6. Data Report: Descriptive Evaluation of Consolidated Sedimentary Rock Structures with X-Ray Imaging: Examples from Site 1276 Core Samples[1]

Masaaki Shirai,[2] Masahiro Nishimura,[3] and Hisato Yasuda[4]

ABSTRACT

In order to evaluate X-ray imaging efficacy for observation and description of sedimentary structures in consolidated sedimentary rocks with a computed tomography (CT) scanner, X-ray images obtained during the Ocean Drilling Program Leg 210 cruise and X-ray CT images obtained during postcruise study are compared with split surface digital images of the correlative half-core.

Sedimentary structures are clearly to faintly recognized with X-ray images, implying that sedimentary rocks (sandstone, siltstone, and shale) retain density contrasts despite decreases in porosity caused by compaction. X-ray imaging is efficient for observing partial sedimentary and postsedimentation structures. However, carbonate rocks tend to be unsuitable for X-ray imaging and observation because whole-core cementation often masks density contrasts, rendering homogeneous sedimentary structures. Overlap of high-angle structures often prevents clear two-dimensional imaging.

X-ray CT scanning is a powerful tool that can image structures in sedimentary rock core samples before they are split. Constructing an efficient X-ray CT imaging methodology to be used during the time constraining the core description process is required.

[1]Shirai, M., Nishimura, M., and Yasuda, H., 2007. Data report: descriptive evaluation of consolidated sedimentary rock structures with X-ray imaging: examples from Site 1276 core samples. *In* Tucholke, B.E., Sibuet, J.-C., and Klaus, A. (Eds.), *Proc. ODP, Sci. Results,* 210: College Station, TX (Ocean Drilling Program), 1–21. doi:10.2973/odp.proc.sr.210.111.2007
[2]Ocean Research Institute, University of Tokyo, 1-15-1 Minamidai, Nakano, Tokyo, 164-8639, Japan. **shirai@ori.u-tokyo.ac.jp**
[3]Marine Works Japan, Yokohama Institute of Marine Science, JAMSTEC, 3172-25 Showa-cho, Kanazawa-ku, Yokohama, 236-0042, Japan.
[4]Center for Advanced Marine Core Research, Kochi University, B200 Monobe, Nankoku, Kochi, 783-8502, Japan.

Initial receipt: 16 February 2006
Acceptance: 26 July 2006
Web publication: 11 May 2007
Ms 210SR-111

INTRODUCTION

X-ray computed tomography (CT) reveals density distributions, which reflect distributions of pores and high atomic number elements within a target using X-ray attenuation. The X-ray beam passing through a sample is attenuated by interaction with the various constituents in the target, and an X-ray CT image is obtained by integrating the X-ray attenuation through 360°. This imaging technique is popular in medical usage and has also become popular in geological usage because it is a nondestructive investigation technique (e.g., Holler and Kögler, 1990; Soh, 1997). X-ray CT imaging can reveal important information about sedimentary structures (e.g., Boespflug et al., 1995), deformation structures (e.g., Soh, 1997), and gas hydrate potential of unconsolidated sediments (Shipboard Scientific Party, 2002).

X-ray CT analyses of consolidated sedimentary rocks have been carried out to image and evaluate pore distributions (e.g., Wellington and Vinegar, 1987; Spanne et al., 1994) and deformation structures (e.g., Soh et al., 1993; Ashi, 1995). To date, X-ray CT studies have not focused on sedimentary structures in consolidated sedimentary rocks. However, we wanted to determine the efficacy of obtaining X-ray CT images of consolidated sedimentary rocks because the new riser drilling platform of the Integrated Ocean Drilling Program, the *Chikyu*, is equipped with a medical CT scanner to be used during the core description process. In this research we evaluated the use of X-ray CT imaging for core observation and description by imaging sedimentary structures in consolidated sedimentary rocks sampled at Ocean Drilling Program Leg 210 Site 1276.

EQUIPMENT

Portable X-Ray CT System on the *JOIDES Resolution*

During Leg 210, a portable X-ray CT system manufactured by Lawrence Berkeley National Laboratory, University of California, was rigged on the *JOIDES Resolution*. The system consists of a core holder in which core is inserted vertically and a gantry holding the X-ray source and detector. The X-ray source has a tungsten target delivering a 130-kV X-ray beam. An X-ray image is displayed on a monitor at 768 × 494 pixels, which converts to a resolution of 0.2 mm × 0.2 mm. During the scan, the core is rotated around its vertical axis and 180 two-dimensional (2-D) X-ray images are acquired at different orientations relative to the core axis. The 2-D images show integrated densities across the entire thickness of the core, so the X-rays penetrating the central part of a core tend to be more heavily attenuated than ones penetrating the right and left sides. The 2-D image set is then stacked to provide a three-dimensional (3-D) density distribution within the core that can be sliced in any orientation for later study. The gantry can be raised and lowered 9 cm by a belt-driven actuator to image selected regions of the core. Details of the imaging process are described in Freifeld et al. (2003) and Shipboard Scientific Party (2004a). Regrettably, the core pieces wobbled in the plastic liner tube during 360° rotation, preventing us from obtaining clear 3-D density distributions. In our study, 2-D X-ray images were therefore used.

Medical X-Ray CT System at Center for Advanced Marine Core Research

As a postcruise study, half-core samples from Site 1276 were imaged using a medical X-ray CT scanner (Radix-Pratico, manufactured by HITACHI Medico, Japan) located at the Center for Advanced Marine Core Research (CMCR) at Kochi University in Japan. A molybdenum-tungsten (Mo-W) metal filament emits a 120-kV X-ray beam. The X-ray emitter and detector rotate around sample on a core holder and acquire a "horizontal (round slice)" 2-D image of the half-core at 512 × 512 pixels, which converts to a resolution of 0.31 mm × 0.31 mm (Hirono et al., 2004) and a slice thickness of 2 mm. The 2-D images acquired at 2-mm intervals were integrated with a processor to construct a 3-D density distribution. Medical scanners can also obtain a vertical 2-D X-ray image of the sample without rotating the gantry.

METHODS

Comparison between 2-D X-Ray Core Image and Digital Image of Split Surface

In order to evaluate efficacy of X-ray CT for observation of sedimentary structures in consolidated sedimentary rocks, the 2-D X-ray images were compared with the split surface digital images of correlative half-core.

As time permitted during routine core handling on Leg 210, various portions of the sections from recovered cores were observed by X-ray CT in 2-D mode and core images were recorded. As described above, the 3-D constructed image was not used. Digital images of correlative half-cores were obtained using the GEOTEK digital imaging system (DIS) on the ship. Details of the DIS are described in Shipboard Scientific Party (2004a). Attitude of the core during imaging (CT = vertical, DIS = horizontal) and core fragmentation resulting from splitting often caused some displacement of features between the two images. Hence, each feature in a DIS image was carefully correlated with the 2-D image based on the positions of cracks, lithological boundaries, and characteristic sedimentary structures. When a sedimentary structure was observed in a digital image, a corresponding structure was sought in the correlative 2-D image and the characteristics of that structure were extracted from the correlative barrel sheet description.

Comparison between 2-D X-Ray Core Image and 3-D CT Core Image

For this comparison, two half-core samples for which a 2-D X-ray image had been obtained during Leg 210 were imaged with the medical X-ray CT scanner at CMCR. In this study, we primarily obtained "vertical" core CT images around the axis for the purpose of comparison with shipboard-acquired 2-D X-ray images.

RESULTS

Comparison between 2-D X-Ray Core Image and Digital Image of Split Surface

A total of 158 portions of whole-core samples were imaged with the portable CT scanner during Leg 210, and 23 2-D X-ray images were compared with digital images of the split surface with good correlation on the basis of cracks, lithologic boundaries, and characteristic sedimentary structures. Herein, we show results of this comparison for 17 samples divided into groups with characteristic sedimentary structures as below. Sampling horizons are shown using those in digital images.

Lamination

Sample 210-1276A-21R-4, 108–117 cm (Fig. **F1A, F1B**), consists of horizontally laminated calcareous sandstone with intrabed folding structures in the upper part of the sample (see 110–111.5 cm in Fig. **F1A**). The X-ray image shows only several dark laminations thicker than ~1 mm. The half-core is broken at thick dark laminae horizons.

Sample 210-1276A-44R-5, 27–36 cm (Fig. **F1C, F1D**), consists of piled trough cross-laminated sandstone. The X-ray image shows laminae thicker than ~1 mm.

Sample 210-1276A-48R-3, 56–65 cm (Fig. **F2A, F2B**), consists of planar-trough cross-laminated sandstone. The X-ray image captured the clear appearance of trough cross-laminae thicker than ~1 mm.

Sample 210-1276A-48R-3, 65–74 cm (Fig. **F2C, F2D**), consists of trough cross-laminated and horizontally laminated sandstone in the upper part of the interval and faintly parallel laminated grainstone in the lower part. The X-ray image clearly captured the upper trough cross-laminae thicker than ~1 mm, whereas the X-ray image of the lower part of the sample is structureless despite coarse-grained mudstone fragments (maximum of ~1.5 mm length) concentrated in layers in the middle and basal parts of the grainstone.

Sample 210-1276A-55R-2, 122–131 cm (Fig. **F3A, F3B**), consists mainly of horizontally laminated sandstone. The lamination varies from ~2 to 0.5 mm thick. In the X-ray image, thin laminae (less than ~0.8 mm thick) cannot be recognized. Thin lamina bundles are recognized as thick laminae in the lower part of the sample (126–129 cm).

Sample 210-1276A-75R-6, 37–46 cm (Fig. **F3C, F3D**), consists of trough cross-laminated grainstone. Although the X-ray image was taken from the same direction with digital image, judging from the appearance of a crack, it does not show any lamination except for a lamina that formed the crack during core splitting.

Sample 210-1276A-89R-4, 103–111 cm (Fig. **F4A, F4B**), consists of parallel laminated sandstone. The laminae vary from 1 to 0.3 mm thick. The X-ray image faintly captures only two thick (8~4 mm) dark-colored beds.

Sample 210-1276A-96R-1, 65–74 cm (Fig. **F4C, F4D**), consists of parallel laminated calcareous sandstone. Discontinuous light-colored laminae and light-colored spots suggest recrystallization of the sandstone. The laminae vary from 2 to 0.5 mm thick. The X-ray image faintly captures several laminae thicker than ~1.5 mm.

F1. Horizontally laminated sandstone and trough cross-laminated sandstone images, p. 10.

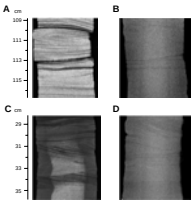

F2. Planar-trough cross-laminated sandstone and laminated sandstone/grainstone images, p. 11.

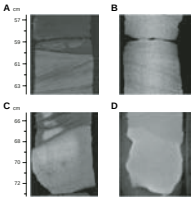

F3. Horizontally laminated sandstone and trough cross-laminated grainstone images, p. 12.

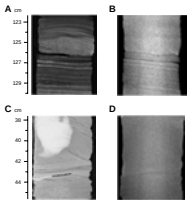

F4. Parallel laminated sandstone and parallel laminated calcareous sandstone images, p. 13.

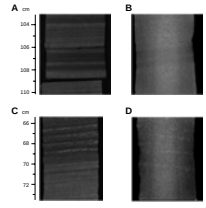

Soft-Sediment Deformation

Sample 210-1276A-53R-3, 0–9 cm (Fig. F5A, F5B), consists of laminated sandstone. The upper part of the sample shows trough cross-lamination and the lower part shows deformed lamination. The difference in the appearance of trough cross-laminae in the two images suggests that the X-ray image and split surface may be offset by 120°–150°. An obscure dark-colored band in the lower part (5–7 cm) of the X-ray image may correspond with thick deformed black laminae.

Sample 210-1276A-60R-1, 76–85 cm (Fig. F5C, F5D), consists of laminated siltstone. Dip angles of the parallel lamination in the lowermost part of the sample suggest that the X-ray image and split surface image are offset by 150°–180°. The lamination is deformed and partially subtle in the X-ray image.

Sample 210-1276A-61R-4, 55–64 cm (Fig. F6A, F6B), consists of laminated sandstone. Dip angles of the parallel lamination in the lower part of the sample and morphology of the intrabed folding suggests that the X-ray image and split surface are offset by ~45°. Soft-sediment deformation (intrabed folding) in the central part of the sample (57–61 cm) is seen clearly in both the DIS and X-ray CT images.

Cementation and Concretion

Sample 210-1276A-61R-2, 47–55 cm (Fig. F7A, F7B), consists of calcareous claystone with lenticular concretions. Two concretions (47 and 50 cm) visible in the X-ray image cannot be seen in the digital image. The upper lenticular concretion would have chipped out during core splitting, and the lower concretion is not exposed on the split surface.

Sample 210-1276A-61R-2, 56–64 cm (Fig. F7C, F7D), consists of calcareous claystone with a lenticular concretion and thin light-colored laminae. A 0.5-mm-thick lamina 2 mm upcore from the concretion (60.3 cm) is recognized on the X-ray image.

Sample 210-1276A-79R-2, 99–108 cm (Fig. F8A, F8B), consists of massive sandstone. The X-ray image shows a sparse distribution of light-colored mottles. A hydrochloric acid test on the splitting surface suggested that these mottles may consist of concreted carbonate minerals.

Sample 210-1276A-91R-3, 13–22 cm (Fig. F8C, F8D), consists of calcareous mudstone. The X-ray image captured a lenticular concretion and a water escape structure that cannot be seen on the digital image of the split surface. The water escape structure may also be filled with calcite.

Other Structures

Sample 210-1276A-1R-2, 90–99 cm (Fig. F9A, F9B), consists of bioturbated massive mudstone. A spiral stringlike structure in the lower part of the X-ray image was difficult to correlate with a corresponding structure on the split surface. The string is possibly a burrow filled with calcite or other minerals. It is notable that horizontal cracks developing on the split surface were not formed on the whole core observed by X-ray imaging. This means that the cracks formed during the core splitting and shows a significant advantage of X-ray observation with a CT scanner.

Sample 210-1276A-89R-6, 95–104 cm (Fig. F9C, F9D), consists of sandstone with convolute lamination and entrained and stretched intraclasts. The X-ray image captured yellowish gray intraclasts and lamination. These structures seem to include pyrite, judging from its color.

F5. Laminated sandstone and laminated siltstone images, p. 14.

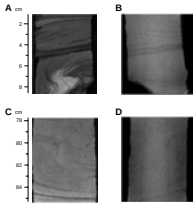

F6. Laminated sandstone images, p. 15.

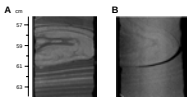

F7. Calcareous claystone images, p. 16.

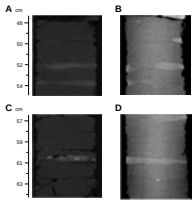

F8. Massive sandstone and calcareous mudstone images, p. 17.

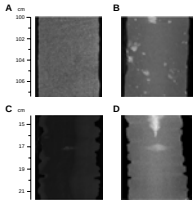

F9. Massive mudstone and sandstone with intraclast images, p. 18.

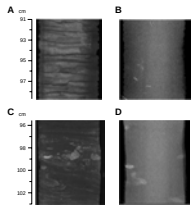

Descriptive features, size (thickness) of the structure in the digital images and in the 2-D X-ray images, lithologic composition, degree of deformation, and estimated offset between the digital and X-ray images are shown in Table **T1.**

T1. Digital image and 2-D X-ray image characteristics, p. 21.

Comparison between 2-D X-Ray Core Image and 3-D CT Core Image

Three-dimensional imaging with a medical CT scanner is time consuming and process intensive. However, it has some merits: (1) structures can be observed from any desired angle, and (2) observation can be limited by selecting a range of CT values. Selecting a range of values increases contrast, making sedimentary structures clearly visible.

Three-dimensional CT images of half-core Sample 210-1276A-44R-5, 27–36 cm, were taken from various directions around the axis of the core at CMCR, and processed in a selected CT value range of 1200–900. This sample corresponds to the sample shown in Figure **F1C** and **F1D.** As the core axis varies, some lamina sets drastically change in visibility. The changes are practically conspicuous in trough cross-laminated portions. Trough cross-lamination in the middle part of the sample is clearly visible in side view (Fig. **F10A–F10C, F10H, F10I**). The same structure in Figure **F10D–F10F, F10J,** and **F10K** is vague and the lamination is not clear. The 2-D X-ray image shown in Figure **F1D** is roughly equivalent to the images shown in Figure **F10I** or **F10J.**

F10. 3-D X-ray CT images of Sample 210-1276A-44R-5, 27–36 cm, p. 19.

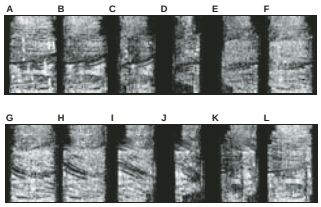

Figure **F11** shows 3-D CT images of Sample 210-1276A-48R-3, 56–65 cm, which corresponds with Figure **F2A** and **F2B** processed in a CT value range of 2100–1800. Visibility of cross-laminae sets changes according to changes in observation direction. Trough cross-lamination in the lower part of the sample is easily distinguished in side view in Figure **F11A, F11B, F11G,** and **F11H.** The same structure in Figure **F11C–F11E, F11J,** and **F11K** is not clear. Lamination in the upper part of the sample appears clearly in Figure **F11E, F11F, F11K,** and **F11L** but is not captured clearly in the Figure **F11B–F11D** and **F11H–F11J.** The 2-D X-ray image shown in Figure **F2B** is roughly equivalent to the one shown in Figure **F11B,** which was taken from a 30° oblique direction.

F11. 3-D X-ray CT images of Sample 210-1276A-48R-3, 56–65 cm, p. 20.

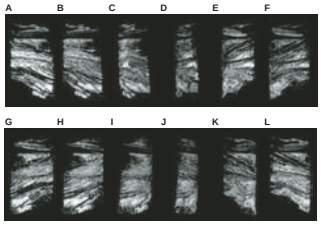

DISCUSSION

Sedimentary structures such as various types of lamination can be clearly to faintly recognized in X-ray images. This implies that the sedimentary rock (sandstone, siltstone, mudstone, and shale) retains density contrasts in spite of the decrease in porosity contrasts caused by compaction. Grain density and porosity profiles (Shipboard Scientific Party, 2004b; fig. F159) show that grain density is consistent throughout the hole and that sandstone and grainstone often have porosities as much as 20% lower than the general trend. Therefore, the density contrast in lamination, which generally consists of repetition of sand-sized grain layers and clay-silt–sized grain layers, is considered to be mainly attributed to remnant of porosity contrast, whereas some sedimentary structures are invisible in X-ray images. This invisibility may be induced by several factors:

1. Resolution of the X-ray image: The threshold thickness of visible/invisible sedimentary structures on 2-D X-ray images is greater than ~0.5 mm (Table **T1**). The minimum thickness of 0.5

mm (Fig. F7D) seems to represent the practical resolution of 2-D images produced by the portable X-ray CT system. In many cases, the minimum thicknesses of sedimentary structures of interest are ~1 mm. Integration of the images across the entire thickness of a core may make the resolution of the X-ray image coarser than the ideal resolution.

2. Whole-rock cementation: Table T1 shows that sedimentary structures in grainstone, marlstone, and calcareous sandstone-siltstone are often invisible on CT images even if the structures are >1 mm thick. The common characteristic of these rocks is that they are cemented by carbonate minerals. Therefore, carbonate cementation may render density distributions that reflect sedimentary structures homogeneous, preventing clear imaging of these sedimentary structures. CT imaging may be more suitable for observation of sedimentary structures in cemented rocks by selecting narrower ranges of CT processing values.
3. Direction of image: Three-dimensional observation of trough cross-lamination from various directions (Figs. F10, F11) shows that side views of the some lamina sets are distinct but at ~90° rotation from the side view laminae are unclear because of overlap. Images of soft-sediment deformation may also be influenced by direction effect. In several cases, intrabed slumps are invisible in 2-D X-ray images (Fig. F5B, F5D) but are clearly observed in another 2-D X-ray image (Fig. F6B). Like cases of high-angle trough cross-laminae, overlap of folded laminae seems to prevent the clear appearance of soft-sediment deformation structures.

On the other hand, X-ray images can reveal sedimentary and postsedimentation structures such as burrows, water escape structures, and small concretions that cannot be seen on the split core surface (Figs. F7, F8, F9, respectively). These structures tends to be filled with authigenic minerals such as calcite and pyrite.

CONCLUSIONS AND PROSPECTS

Sedimentary structures are recognized on 2-D X-ray images, implying that sedimentary rocks (sandstone, siltstone, mudstone, and shale) retain density contrast in spite of decreases in porosity caused by its compaction. X-ray CT is a powerful tool that can reveal important information about structures of consolidated sedimentary rock core samples before splitting, even if only 2-D X-ray imaging is used. X-ray imaging is an efficient method of observing partial sedimentary and postsedimentation structures such as burrows, water escape structures, and small concretions that are often not recognized with split surface observation. CT scanning just after coring may be efficient to describe unstable minerals. Carbonate rocks tend to be unsuitable for X-ray imaging and observation because whole-core cementation often obscures density contrasts, rendering sedimentary structures homogeneous. This is a problem for future studies.

Core imaging from various directions is important for observation of high-angle structures such as trough cross-laminae and intrabed slumps because overlapping structures often prevent clear imaging from a single direction. Hence, it is valuable to construct a system of CT observation and image analysis before core splitting. Core splitting in an appropriate direction will improve accuracy of description and sampling. Because of

time constraints inherent in core handling, an effective and efficient X-ray CT procedure must be constructed as a part of the core description process. At a minimum, the procedure should include: (1) 2-D X-ray imaging of the core from several different directions, (2) rough evaluation of sedimentary structures, and (3) determination of the best direction for core splitting.

ACKNOWLEDGMENTS

We thank our colleagues on Leg 210 and the crew of the *JOIDES Resolution* for helpful advice and skillful operations. William Mills, Johanna Suhonen, and Patrick Riley are particularly thanked for helping operate the CT scanner and analysis software XVIEW on board the *JOIDES Resolution*. We also thank Dr. Barry M. Freifeld for his lecture on operating the portable CT scanner on the *JOIDES Resolution* and Dr. O. Tadai for his help operating the medical CT scanner at the CMCR, Koch University. Our manuscript was improved by Lorri Peters and anonymous reviewers.

This research used samples and data provided by the Ocean Drilling Program (ODP). ODP is sponsored by U.S. National Science Foundation (NSF) and participating countries under management of Joint Oceanographic Institution (JOI), Inc.

REFERENCES

Ashi, J., 1995. CT scan analysis of sediments from Leg 146. *In* Carson, B., Westbrook, G.K., Musgrave, R.J., and Suess, E. (Eds.), *Proc. ODP, Sci. Results,* 146 (Pt 1): College Station, TX (Ocean Drilling Program), 191–199. **doi:10.2973/odp.proc.sr.146-1.214.1995**

Boespflug, X., Long, B.F.N., and Occhietti, S., 1995. CAT-scan in marine stratigraphy: a quantitative approach. *Mar. Geol.,* 122(4):281–301. **doi:10.1016/0025-3227(94)00129-9**

Freifeld, B.M., Kneafsey, T.J., Tomutsa, L, and Pruess, J., 2003. Development of a portable X-ray computed tomographic imaging system for drill-site investigation of recovered core. *Proc. Int. Symp. Soc. Core Anal., September 21–24, 2003, Pau, France,* 581–586.

Hirono T., Nishimura, M., Takemura, T., Soh, W., Murayama, M., and Yasuda, H., 2004. Accuracy check of grading on the medical XCT system. *J. Geol. Soc. Japan,* 110:552–556.

Holler, P., and Kögler, F.-C., 1990. Computer tomography: a nondestructive, high-resolution technique for investigation of sedimentary structures. *Mar. Geol.,* 91(3):263–266. **doi:10.1016/0025-3227(90)90041-H**

Shipboard Scientific Party, 2002. Leg 204 preliminary report. *ODP Prelim. Rpt.,* 204 [Online]. Available from World Wide Web: <**http://www-odp.tamu.edu/publications/prelim/204_prel/204PREL.PDF**>. [Cited 2003-08-30]

Shipboard Scientific Party, 2004a. Explanatory notes. *In* Tucholke, B.E., Sibuet, J.-C., Klaus, A., et al., *Proc. ODP, Init. Repts.,* 210: College Station, TX (Ocean Drilling Program), 1–69. **doi:10.2973/odp.proc.ir.210.102.2004**

Shipboard Scientific Party, 2004b. Site 1276. *In* Tucholke, B.E., Sibuet, J.-C., Klaus, A., et al., *Proc. ODP, Init. Repts.,* 210: College Station, TX (Ocean Drilling Program), 1–358. **doi:10.2973/odp.proc.ir.210.103.2004**

Soh, W., 1997. Computed tomography scan analysis of Site 941 cores, western mass-transport deposit, Amazon Fan. *In* Flood, R.D., Piper, D.J.W., Klaus, A., and Peterson, L.C. (Eds.), *Proc. ODP, Sci. Results,* 155: College Station, TX (Ocean Drilling Program), 465–475. **doi:10.2973/odp.proc.sr.155.231.1997**

Soh, W., Byrne, T., Taira, A., and Kono, A., 1993. Computed tomography (CT) scan image analysis of Site 808 cores: structural and physical property implications. *In* Hill, I.A., Taira, A., Firth, J.V., et al., *Proc. ODP, Sci. Results,* 131: College Station, TX (Ocean Drilling Program), 135–140. **doi:10.2973/odp.proc.sr.131.113.1993**

Spanne, P., Thovert, J.F., Jacquin, C.J., Lindquist, W.B., Jones, K.W., and Adler, P.M., 1994. Synchrotron computed microtomography of porous media: topology and transports. *Phys. Rev. Lett.,* 73(14):2001–2004. **doi:10.1103/PhysRevLett.73.2001**

Wellington, S.L., and Vinegar, H.J., 1987. X-ray computerized tomography. *J. Pet. Technol.,* 39:885–898.

Figure F1. A, B. Horizontally laminated calcareous sandstone (Sample 210-1276A-21R-4, 108–117 cm); (A) digital image of split surface; (B) 2-D X-ray image. Split surface and X-ray images are taken from similar directions. **C, D.** Trough cross-laminated sandstone (Sample 210-1276A-44R-5, 27–36 cm); (C) digital image of split surface; (D) 2-D X-ray image. Split surface and X-ray images may be offset by 90° or more.

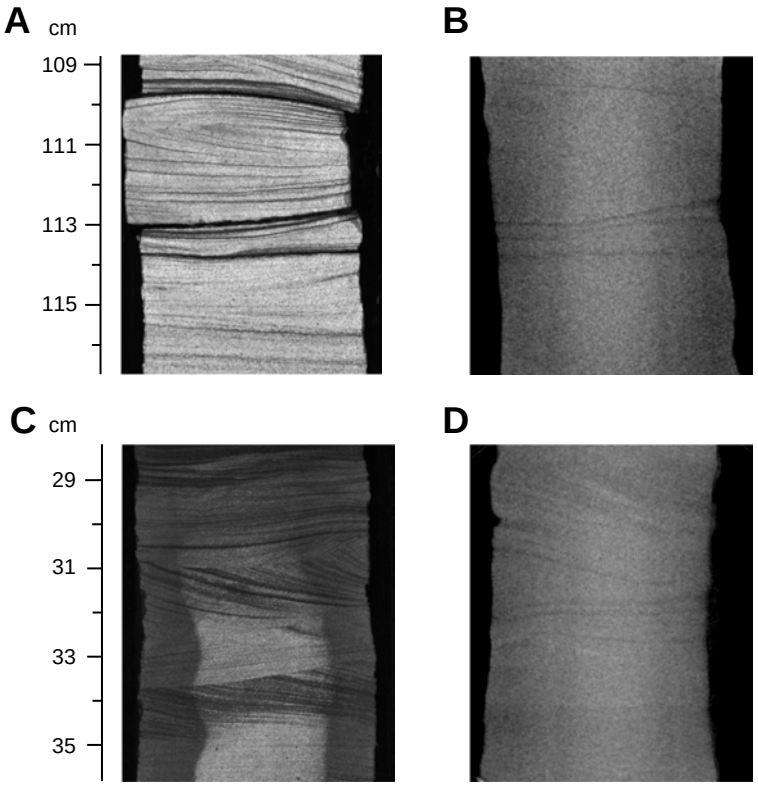

Figure F2. A, B. Planar-trough cross-laminated sandstone (Sample 210-1276A-48R-3, 56–65 cm); (A) digital image of split surface; (B) 2-D X-ray image. Split surface and X-ray images are offset by >90°. **C, D.** Laminated sandstone/grainstone (Sample 210-1276A-48R-3, 65–74 cm); (C) digital image of split surface; (D) 2-D X-ray image. Split surface and X-ray images are offset by >90°.

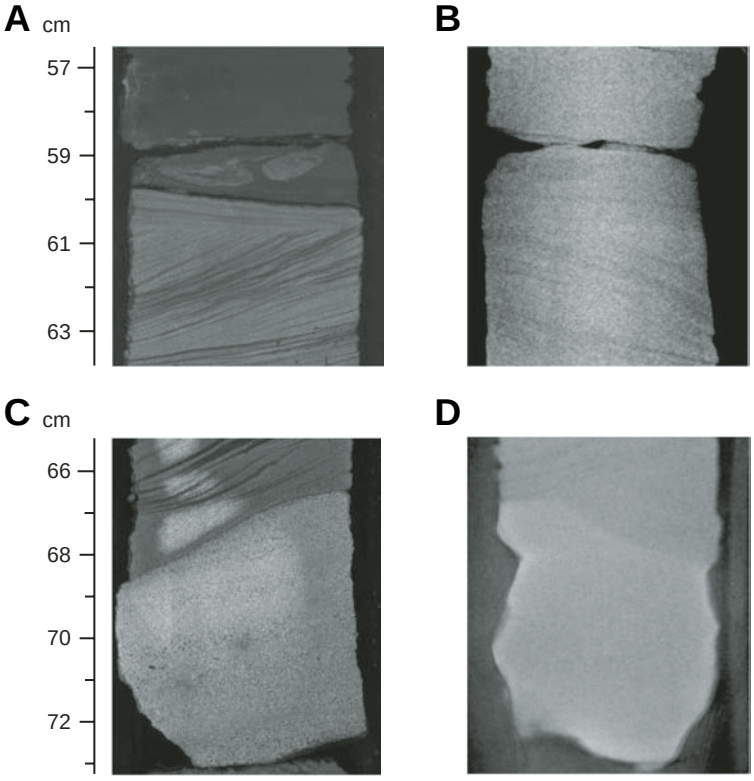

Figure F3. A, B. Horizontally laminated sandstone (Sample 210-1276A-55R-2, 122–131 cm); (A) digital image of split surface; (B) 2-D X-ray image. Split surface and X-ray images are taken from similar directions. **C, D.** Trough cross-laminated grainstone (Sample 210-1276A-75R-6, 37–46 cm); (C) digital image of split surface; (D) 2-D X-ray image. Split surface and X-ray image are taken from similar directions.

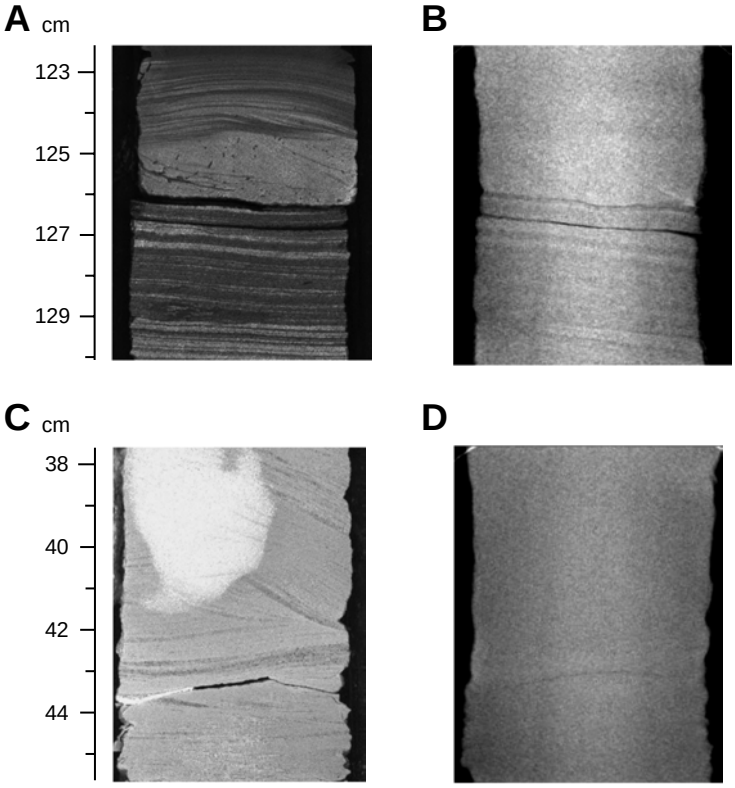

Figure F4. A, B. Parallel laminated sandstone (Sample 210-1276A-89R-4, 103–111 cm); (A) digital image of split surface; (B) 2-D X-ray image. Offset in direction between the two images is unknown. **C, D.** Parallel laminated calcareous sandstone (Sample 210-1276A-96R-1, 65–74 cm); (C) digital image of split surface; (D) 2-D X-ray image. Offset in direction between the two images is unknown.

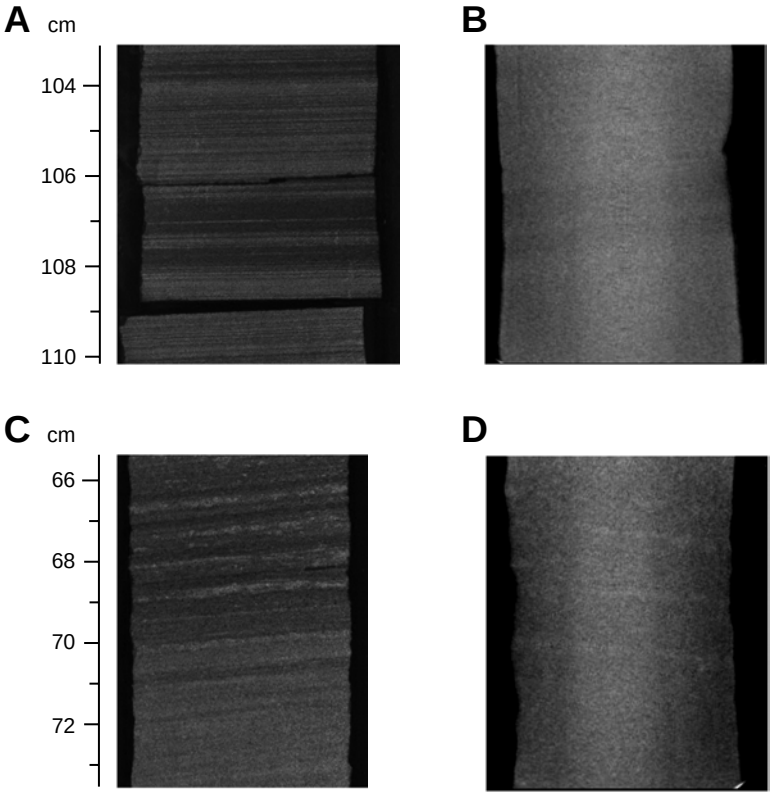

Figure F5. A, B. Laminated sandstone (Sample 210-1276A-53R-3, 0–9 cm); (A) digital image of split surface; (B) 2-D X-ray image. Split surface and X-ray images are offset by >90°. **C, D.** Laminated siltstone (Sample 210-1276A-60R-1, 76–85 cm); (C) digital image of split surface; (D) 2-D X-ray image. Split surface and X-ray images are offset by almost 180°.

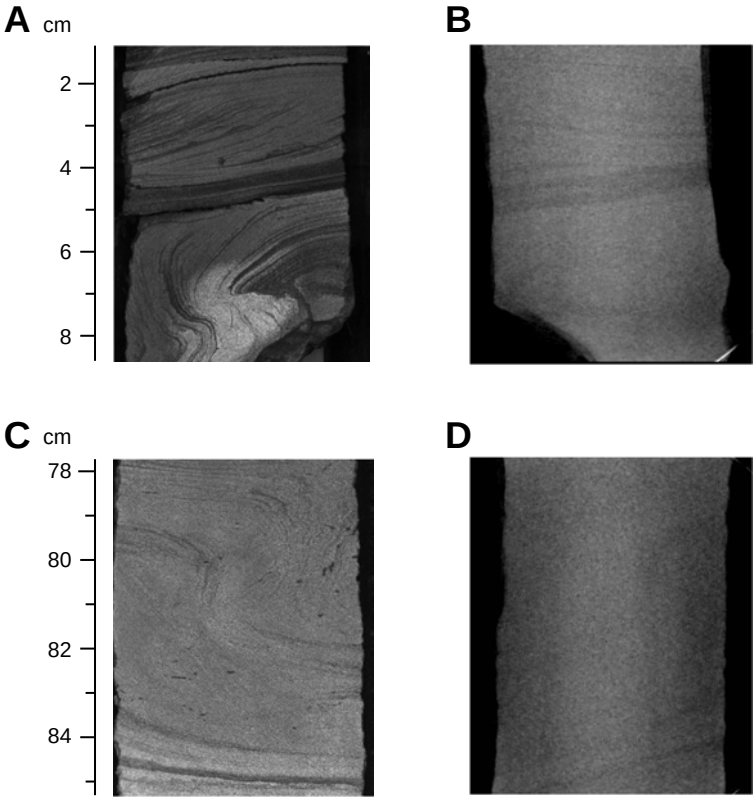

Figure F6. A, B. Laminated sandstone (Sample 210-1276A-61R-4, 55–64 cm); (A) digital image of split surface; (B) 2-D X-ray image. Split surface and X-ray images are offset by ~45°.

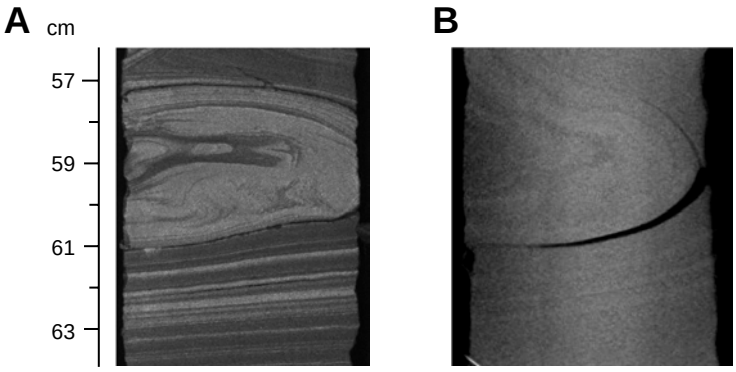

Figure F7. A, B. Calcareous claystone (Sample 210-1276A-61R-2, 47–55 cm); (A) digital image of split surface; (B) 2-D X-ray image. Split surface and CT images are offset by 90° or more. **C, D.** Calcareous claystone (Sample 210-1276A-61R-2, 56–64 cm); (C) digital image of split surface; (D) 2-D X-ray image. Split surface and X-ray images are offset by 90° or more because C and D correlate with A and B, respectively.

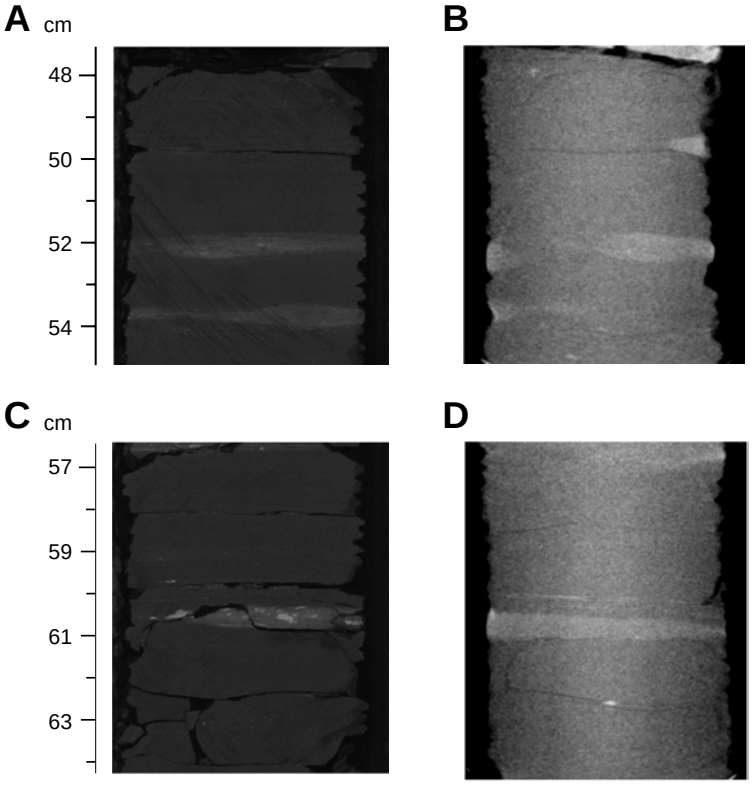

Figure F8. A, B. Massive sandstone (Sample 210-1276A-79R-2, 99–108 cm); (A) digital image of split surface; (B) 2-D X-ray image. Offset in direction between the two images is unknown. **C, D.** Calcareous mudstone (Sample 210-1276A-91R-3, 13–22 cm); (C) digital image of split surface; (D) 2-D X-ray image. Offset in direction between the two images is unknown.

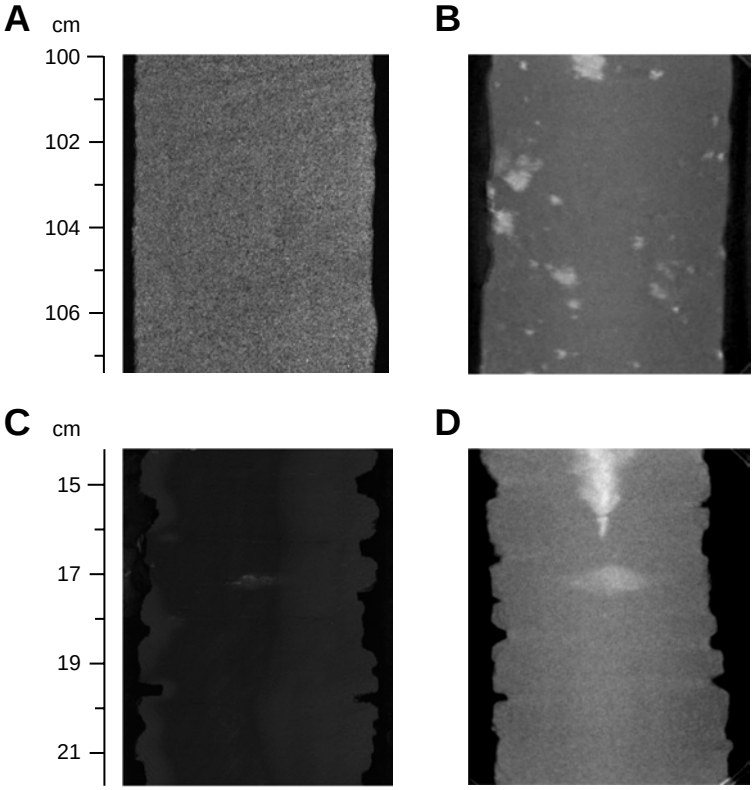

Figure F9. A, B. Massive mudstone (Sample 210-1276A-1R-2, 90–99 cm); (A) digital image of split surface; (B) 2-D X-ray image. Offset in direction between the two images is unknown. The relative positions of A and B are not correlated rigidly due to lack of key horizons. **C, D.** Sandstone with intraclast (Sample 210-1276A-89R-6, 95–104 cm); (C) digital image of split surface; (D) 2-D X-ray image. Split surface and X-ray images are taken from similar directions.

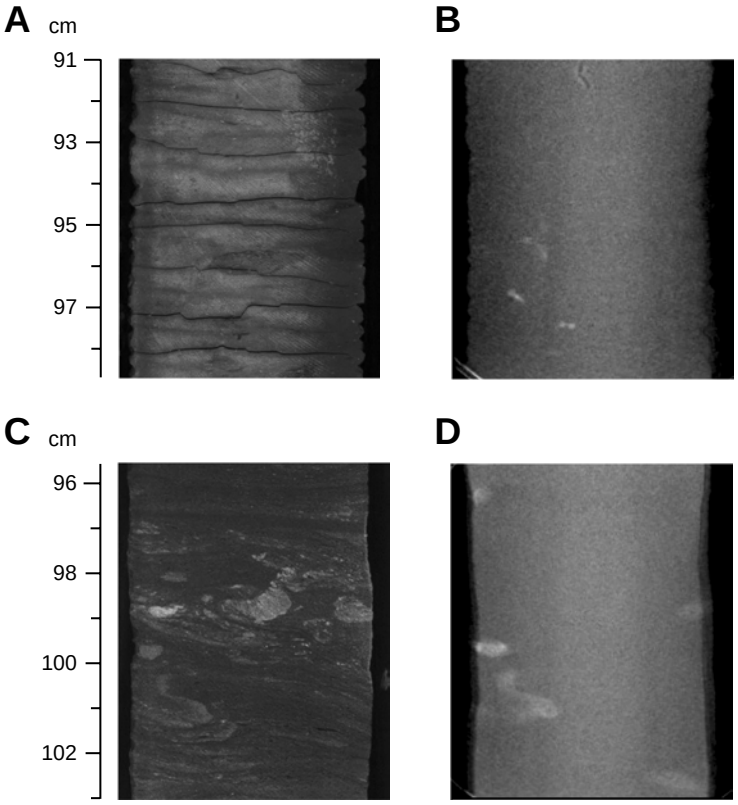

Figure F10. Three-dimensional X-ray CT images of half-core Sample 210-1276A-44R-5, 27–36 cm, which is the same sample shown in Figure F1C and F1D, p. 10. Core image is rotated at 30° steps from A to L.

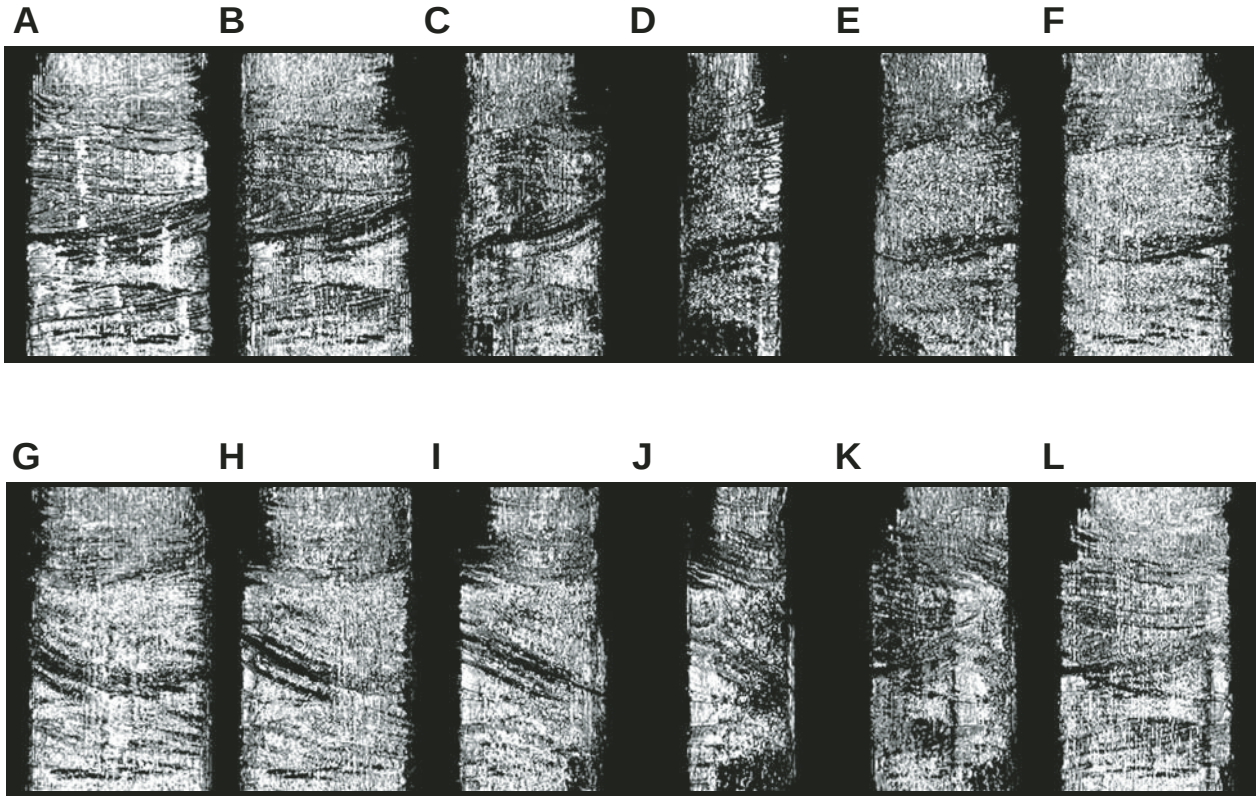

Figure F11. Three-dimensional X-ray CT images of half-core Sample 210-1276A-48R-3, 56–65 cm, which is the same sample shown in Figure F2A and F2B, p. 11. Core image is rotated at 30° steps from A to L.

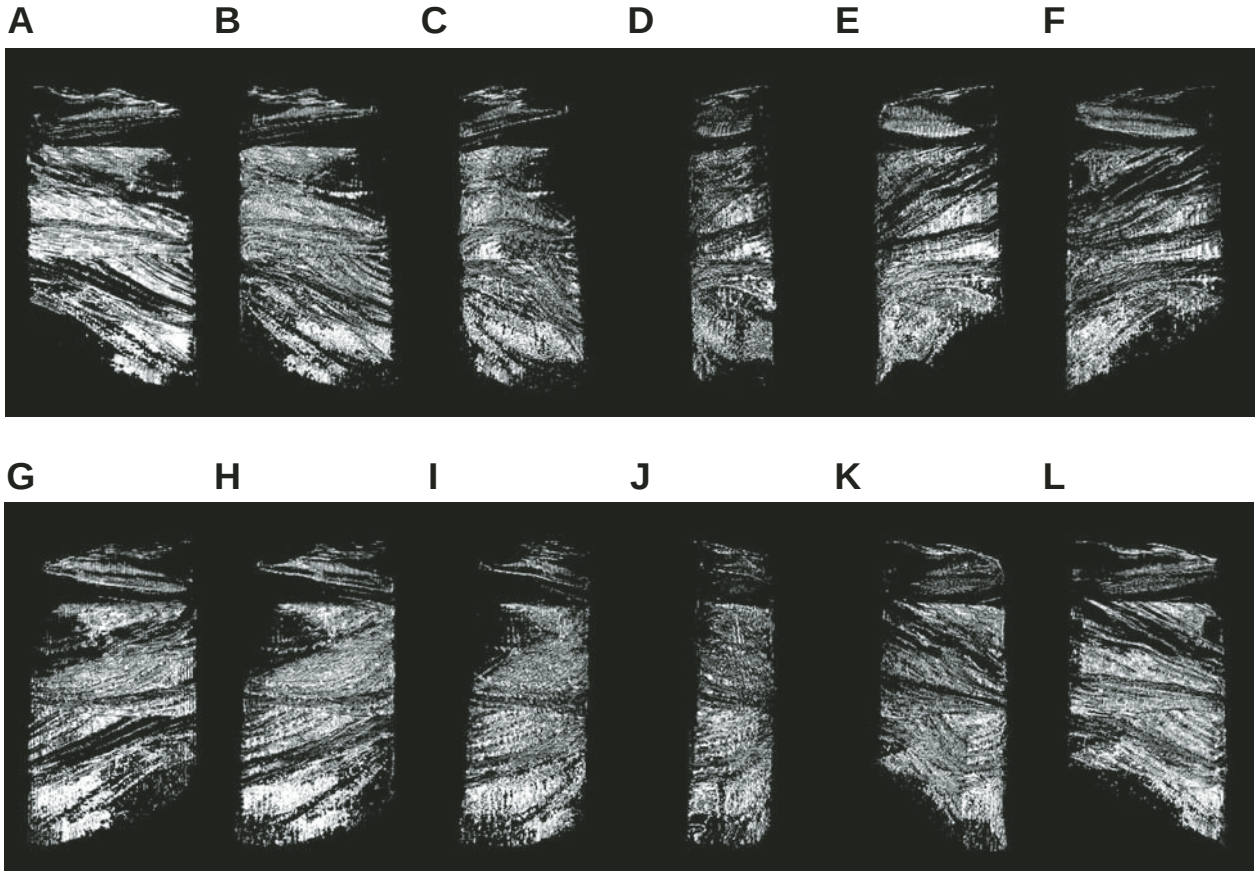

Table T1. Summary of digital image and two-dimensional (2-D) X-ray image characteristics of 23 samples in which stratigraphic position of both images are correlated well.

Core, section, interval (cm)	Descriptive features	Size of structure (mm)	Detectable size of str. in 2-D CT (mm)	Lithology	Deformation	Offset in direction (°)	
207-1276A-							
1R-2, 90–99	Spiral string (burrow?)	(Massive)	~1	Mudstone	No	?	Figure **F9A** and **F9B**
21R-4, 108–117	Cross and deformed lam.	2~0.5	~1	Calcareous SST	Partial	<30	Figure **F1A** and **F1B**
44R-5, 27–36	Trough cross lam.	2~0.5	~1	SST	No	90–120?	Figures **F1C**, **F1D**, and **F10**
48R-3, 56–65	P. lam. and t. c. lam.	1~0.5	~1	SST	No	120–150	Figures **F2A**, **F2B**, and **F11**
48R-3, 65–74(u)	Trough c. lam.	2~0.5	~1	SST	No	120–150	Figure **F2C** and **F2D**
48R-3, 65–74(l)	Cross lam.	1.5~0.5	(Invisible)	Grainstone	No	120–150	Figure **F2C** and **F2D**
53R-3, 0–9(u)	Cross lam.	4~0.8	~1	SST	No	120–150	Figure **F5A** and **F5B**
53R-3, 0–9(l)	Deformed lam.	2~0.5	(Invisible)	SST	Heavy	120–150	Figure **F5A** and **F5B**
55R-2, 122–131	P. lam. (Partially c. lam.)	2~0.5	0.8	SST	No?	<30	Figure **F3A** and **F3B**
60R-1, 76–85	Deformed lam.	3~0.8	~2	SLST with sandy lam.	Heavy	150–180?	Figure **F5C** and **F5D**
61R-2, 47–55	Concretion	4~2	4~2	Calcareous CST	No	90–120	Figure **F7A** and **F7B**
61R-2, 56–64	Concretion	2~0.5	2~0.5	Shale	No	90–120	Figure **F7C** and **F7D**
61R-2, 138–147	Deformation	1–1.5	(Invisible)	Calcareous SLST	Heavy	60–120?	
61R-4, 55–64	Deformation	4~0.5	~1	SST	Heavy	30–60	Figure **F6A** and **F6B**
75R-6, 37–46	Trough c. lam.	2~0.5	(Invisible)	Grainstone	No	<30	Figure **F3C** and **F3D**
75R-6, 81–90	P. lam.	(~1)	(~1)	Marlstone	No	<30	
77R-1, 0–9	Lith. frag. in massive SST	1~2	(Invisible)	Silty SST	Little	?	
77R-4, 72–81	Burrow (mud pipe)	~1	(Invisible)	SLST-shale	No	?	
79R-2, 99–108	Concretion	(Massive)	(8~0.5)	SST	No	?	Figure **F8A** and **F8B**
89R-4, 103–111	P. lam.	5~0.5	4	SST	No	?	Figure **F4A** and **F4B**
89R-6, 45–54	Whirl lam.	3~0.5	3~1	SST-marlstone	Heavy	?	
89R-6, 95–104	Concretion	5~0.5	5~1	SST	Considerable	<30	Figure **F9C** and **F9D**
91R-3, 13–22	Water escape and concretion	(>4)	(7~1)	Shale	No	?	Figure **F8C** and **F8D**
92R-5, 117–126	P. lam.	3~0.5	2~0.5	Calcareous SST	Little?	60–120?	
96R-1, 65–74	P. lam.	2~0.5	~2	Calcareous SST-SLST	No	?	Figure **F4C** and **F4D**

Notes: Descriptive features, size (thickness) of the structure in digital image and 2-D X-ray image, lithologic composition, degree of deformation, and estimated difference in directions of digital and X-ray images are shown. CT = computed tomography. SST = sandstone, SLST = siltstone, CST = claystone, lam = lamination. ? = unknown.